

Article

# Formation of $\text{Mo}_5\text{Si}_3/\text{Mo}_3\text{Si}-\text{MgAl}_2\text{O}_4$ Composites via Self-Propagating High-Temperature Synthesis

Chun-Liang Yeh \* and Yin-Chien Chen

Department of Aerospace and Systems Engineering, Feng Chia University, Taichung 40724, Taiwan; m0626603@fcu.edu.tw

\* Correspondence: clyeh@fcu.edu.tw; Tel.: +886-4-2451-7250 (ext. 3963)

Received: 21 November 2019; Accepted: 23 December 2019; Published: 24 December 2019



**Abstract:** In situ formation of intermetallic/ceramic composites composed of molybdenum silicides ( $\text{Mo}_5\text{Si}_3$  and  $\text{Mo}_3\text{Si}$ ) and magnesium aluminate spinel ( $\text{MgAl}_2\text{O}_4$ ) was conducted by combustion synthesis with reducing stages in the mode of self-propagating high-temperature synthesis (SHS). The SHS process combined intermetallic combustion between Mo and Si with metallothermic reduction of  $\text{MoO}_3$  by Al in the presence of MgO. Experimental evidence showed that combustion velocity and temperature decreased with increasing molar content of  $\text{Mo}_5\text{Si}_3$  and  $\text{Mo}_3\text{Si}$ , and therefore, the flammability limit determined for the reaction at  $\text{Mo}_5\text{Si}_3$  or  $\text{Mo}_3\text{Si}/\text{MgAl}_2\text{O}_4 = 2.0$ . Based upon combustion wave kinetics, the activation energies,  $E_a = 68.8$  and  $63.8$  kJ/mol, were deduced for the solid-state SHS reactions producing  $\text{Mo}_5\text{Si}_3-$  and  $\text{Mo}_3\text{Si}-\text{MgAl}_2\text{O}_4$  composites, respectively. Phase conversion was almost complete after combustion, with the exception of trivial unreacted Mo existing in both composites and a minor amount of  $\text{Mo}_3\text{Si}$  in the  $\text{Mo}_5\text{Si}_3-\text{MgAl}_2\text{O}_4$  composite. Both composites display a dense morphology formed by connecting  $\text{MgAl}_2\text{O}_4$  crystals, within which micro-sized molybdenum silicide grains were embedded. For equimolar  $\text{Mo}_5\text{Si}_3-$  and  $\text{Mo}_3\text{Si}-\text{MgAl}_2\text{O}_4$  composites, the hardness and fracture toughness are 14.6 GPa and  $6.28 \text{ MPa m}^{1/2}$ , and 13.9 GPa and  $5.98 \text{ MPa m}^{1/2}$ , respectively.

**Keywords:** intermetallic/ceramic composite; self-propagating high-temperature synthesis;  $\text{Mo}_5\text{Si}_3$ ;  $\text{Mo}_3\text{Si}$ ;  $\text{MgAl}_2\text{O}_4$

## 1. Introduction

Transition metal silicides are considered as a unique class of intermetallic compounds for ultra-high-temperature applications. In the Mo–Si binary system, there exist three silicides— $\text{MoSi}_2$ ,  $\text{Mo}_5\text{Si}_3$ , and  $\text{Mo}_3\text{Si}$ . Among them,  $\text{Mo}_5\text{Si}_3$  with a melting point of  $2180$  °C is the most refractory and  $\text{MoSi}_2$  is the most studied phase.  $\text{MoSi}_2$  has relatively low density, excellent oxidation and corrosion resistance, high thermal and electric conductivities, and good compatibility with many ceramic reinforcements [1,2]. Recently,  $\text{Mo}_5\text{Si}_3$  has attracted growing interests not only due to its high melting point, but also because of its large alloying potential, wide homogeneity range, high strength, and creep resistance superior to  $\text{MoSi}_2$  [3,4].  $\text{Mo}_3\text{Si}$  is an important structural material as well, especially in the development of  $\alpha\text{-Mo}-\text{Mo}_5\text{SiB}_2-\text{Mo}_3\text{Si}$  composites [5,6]. Because silicides and ceramics are two sorts of high-temperature materials highly synergistic with each other, mechanical properties of silicide intermetallics can be effectively improved by the addition of ceramic phases [7–9].

Magnesium aluminate spinel ( $\text{MgAl}_2\text{O}_4$ ) possesses many advantageous properties, including high hardness (16.1 GPa), high melting point ( $2135$  °C), relatively low density ( $3.58 \text{ g/cm}^3$ ), high chemical inertness, low thermal expansion coefficient, high mechanical strength, and good thermal shock resistance [10,11]. However, both conventional solid-state reaction and wet chemical methods

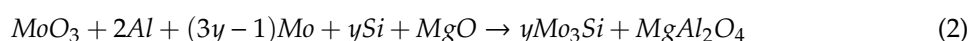
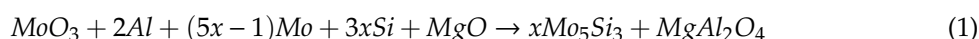
require lengthy processing time and complicated synthesis steps to obtain  $\text{MgAl}_2\text{O}_4$  with specific characteristics [12–14].

Because ceramic-added  $\text{MoSi}_2$  has been extensively investigated, this study aims to prepare molybdenum silicides ( $\text{Mo}_5\text{Si}_3$  and  $\text{Mo}_3\text{Si}$ ) and  $\text{MgAl}_2\text{O}_4$  composites by a facile fabrication route involving solid-phase combustion reaction with metallothermic reduction. The synthesis reaction was formulated with sufficient energy release to proceed in the self-propagating high-temperature synthesis (SHS) mode. The SHS process has the merits of high energy effectiveness, short reaction time, simple operation, and good purification capability [15–17]. Aluminothermic reduction of metal oxides is thermally beneficial for combustion synthesis of materials with low formation enthalpies and provides in situ generation of  $\text{Al}_2\text{O}_3$  [18–20]. The SHS reaction combined with aluminothermic reduction was conducted with green compacts made up of  $\text{MoO}_3$ ,  $\text{SiO}_2$ , Al, and  $\text{MgO}$  for the synthesis of  $\text{MoSi}_2$ - and  $\text{Mo}_5\text{Si}_3$ - $\text{MgAl}_2\text{O}_4$  composites [21]. According to Zaki et al. [21], it required excess  $\text{MoO}_3$  to compensate for its volatilization loss and a higher reaction pressure to suppress the vaporization of  $\text{MoO}_3$ . Horvitz and Gotman [22] performed combustion synthesis in both SHS and thermal explosion modes using powder compacts of  $2\text{TiO}_2$ - $\text{Mg}$ - $4\text{Al}$  to fabricate  $\text{Al}_2\text{O}_3$ -rich spinel and two aluminides— $\text{TiAl}$  and  $\text{Ti}_3\text{Al}$ . Recently, Omran et al. [23] studied reduction of  $\text{WO}_3$  and  $\text{B}_2\text{O}_3$  by Mg in the presence of  $\text{Al}_2\text{O}_3$  to prepare  $\text{MgAl}_2\text{O}_4$ -W and  $\text{MgAl}_2\text{O}_4$ -W- $\text{W}_2\text{B}$  composites in the SHS manner. As proposed by Omran et al. [23],  $\text{MgAl}_2\text{O}_4$  was formed through dissolution of  $\text{MgO}$  into the  $\text{Al}_2\text{O}_3$  melt.

On in situ formation of  $\text{MgAl}_2\text{O}_4$  and  $\text{Mo}_5\text{Si}_3$  or  $\text{Mo}_3\text{Si}$  composites, this study explores the influence of the stoichiometry of reactants on the flammability limit and combustion wave kinetics of the SHS reaction. The phase composition and microstructure of the final products were characterized and the hardness and fracture toughness were examined.

## 2. Materials and Methods

The starting materials included  $\text{MoO}_3$  (Acros Organics, 99.5%, Waltham, MA, USA), Mo (Strem Chemicals, <45  $\mu\text{m}$ , 99.9%, Newburyport, MA, USA), Al (Showa Chemical Co., <45  $\mu\text{m}$ , 99.9%, Tokyo, Japan), Si (Strem Chemicals, <45  $\mu\text{m}$ , 99.5%), and  $\text{MgO}$  (Alfa Aesar, 99%, Ward Hill, MA, USA). Two reaction systems, formulated below, were composed of the Al- $\text{MoO}_3$  thermite and Mo, Si, and  $\text{MgO}$  for the synthesis of  $\text{Mo}_5\text{Si}_3$ - and  $\text{Mo}_3\text{Si}$ - $\text{MgAl}_2\text{O}_4$  composites.



where stoichiometric coefficients,  $x$  and  $y$ , in Reactions (1) and (2) signify  $\text{Mo}_5\text{Si}_3$  and  $\text{Mo}_3\text{Si}$  produced per unit mole of  $\text{MgAl}_2\text{O}_4$  in the composites.

Within two thermite-containing SHS systems, the  $\text{MoO}_3 + 2\text{Al}$  reaction is extremely energetic with the reaction heat of  $\Delta H = -930.7$  kJ and an adiabatic temperature of  $T_{ad} = 4280$  K [24]. However, formation enthalpies of  $\text{Mo}_5\text{Si}_3$  and  $\text{Mo}_3\text{Si}$  (i.e.,  $\Delta H_f = -310.6$  and  $-118.4$  kJ/mol [25]) are much lower than the heat released from the  $\text{MoO}_3 + 2\text{Al}$  thermite. The addition of Mo, Si, and  $\text{MgO}$  has a dilution effect on the combustion reaction. Moreover, the adiabatic temperatures of intermetallic reactions between Mo and Si to form  $\text{Mo}_5\text{Si}_3$  and  $\text{Mo}_3\text{Si}$  are lower than the criterion temperature (1800 K) required for self-sustaining combustion [15]. Therefore, it is believed that in the reaction mechanisms, aluminothermic reduction of  $\text{MoO}_3$  is the initiation step.

The adiabatic combustion temperatures ( $T_{ad}$ ) associated with Reactions (1) and (2) under different stoichiometric coefficients were calculated according to the following equation [21,26] with thermochemical data taken from [25]:

$$\Delta H_r + \int_{298}^{T_{ad}} \sum n_j C_p(P_j) dT + \sum_{298-T_{ad}} n_j L(P_j) = 0 \quad (3)$$

where  $\Delta H_r$  is the reaction enthalpy at 298 K,  $n_j$  is the stoichiometric constant,  $C_p$  and  $L$  are the heat capacity and latent heat, and  $P_j$  refers to the product.

The SHS experiments were conducted in a combustion chamber equipped with quartz viewing windows and filled with high-purity (99.99%) argon. The reactant powders were mixed in a ball mill. Then, the powder mixture was uniaxially compressed in a stainless-steel mold at a pressure of 60–70 MPa to form cylindrical test specimens 7 mm in diameter, 12 mm in height, and with a relative density of 60%. The propagation velocity of combustion wave ( $V_f$ ) was determined from the time series of recorded combustion images. The reaction temperature was measured by a bare wire Pt/Pt–13%Rh thermocouple with a bead diameter of 125  $\mu\text{m}$ . In this study, a two-hole ceramic protection tube was used to accommodate the fine wire thermocouple. The junction was exposed outside the protection tube and the length of the wire protruding from the tube was only about 3 mm. Because the ceramic tube was well mounted and the protruding length was short, the whole setup was rigid and the thermocouple bead had good contact with the sample. Details of the experimental scheme were described elsewhere [27].

According to Bradley and Matthews [28], the conduction loss from the thermocouple depends on the length of wire between the junction and the support. The thermocouple used in this study was 40 mm in length and 62.5  $\mu\text{m}$  in wire diameter. This dimension justifies the measurement practically unaffected by the conduction cooling [28]. However, the radiation loss from the thermocouple bead is another source of error in the thermocouple measurement. An estimate of the radiation correction can be obtained by assuming that a steady state exists between convective heat transfer to and radiation loss from the thermocouple bead [29].

$$\Delta T = \frac{\sigma \cdot \varepsilon \cdot D}{Nu \cdot k} (T_c^4 - T_\infty^4) \quad (4)$$

where  $\sigma$  is the Stefan–Boltzmann constant,  $\varepsilon$  the thermocouple emissivity,  $D$  the thermocouple bead diameter,  $Nu$  the Nusselt number, and  $k$  the gas thermal conductivity.

Product constituents were analyzed by an X-ray diffractometer (Bruker D2, Billerica, MA, USA) using  $\text{CuK}\alpha$  radiation. Examination of the microstructure and elemental proportion of the composite was performed by a scanning electron microscope (Hitachi S3000H, Tokyo, Japan) and energy dispersive spectroscopy (EDS). Moreover, Vickers hardness ( $H$ ) and fracture toughness ( $K_{IC}$ ) of the final products were measured [30,31]. For the hardness and fracture toughness measurement, the selected experiments of Reaction (1) with  $x = 1.0$  and Reaction (2) with  $y = 1.0$  were conducted by placing the powder compact in a steel mold. Densification of the product was accomplished by a hydraulic press machine. Upon completion of the self-sustaining combustion reaction, the burned sample was quickly pressed when the product was still hot and plastic, which was held for about 15 s. The density of the pressed products reached about 98% of theoretical density. The surface of the specimens was then polished for the measurement.

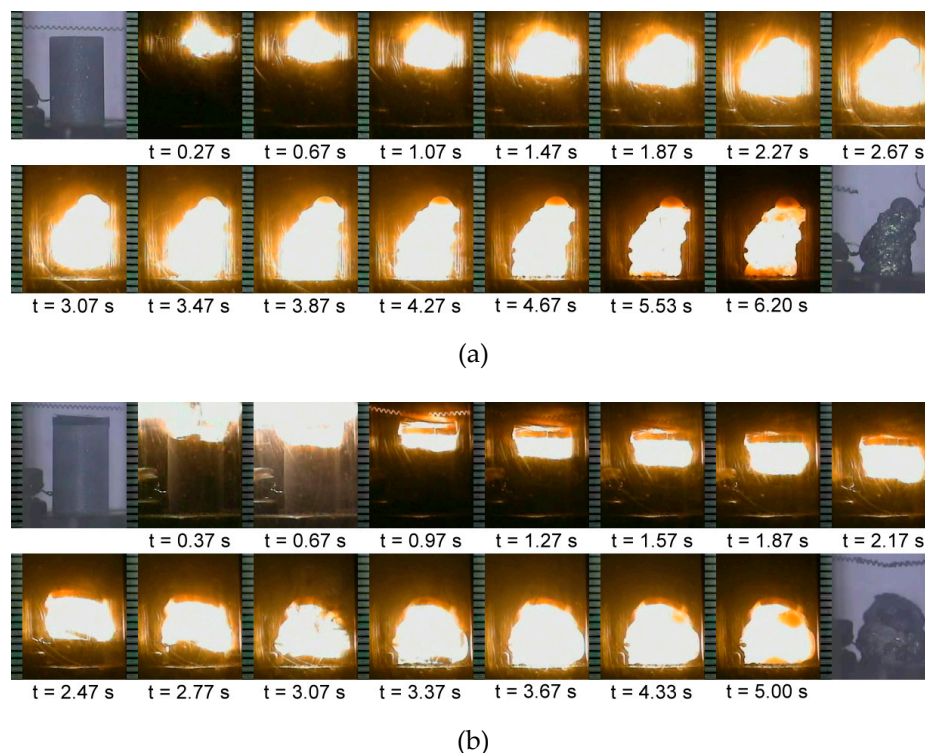
### 3. Results and Discussion

#### 3.1. Combustion Wave Kinetics and Activation Energy

Figure 1a,b presents typical sequences of combustion pictures recorded from Reactions (1) and (2), respectively, and shows that upon ignition, self-sustaining combustion is established. With the progression of combustion wave, as illustrated in Figure 1, the reacted samples are partially molten and shrunk. Sample shrinkage during the SHS process was due perhaps to the low melting points of thermite reagents (795 °C for  $\text{MoO}_3$  and 660 °C for Al). The presence of liquid melt contributed to self-densification of the final product. As mentioned above, reaction exothermicity tends to weaken with increasing molar content of molybdenum silicides. Based on experimental evidence, the flammability limits of Reactions (1) and (2) in terms of their stoichiometric coefficients exist at  $x = 2.0$  and  $y = 2.0$ , respectively. That is, combustion ceased to propagate and quenched as long as the stoichiometric coefficient of the reaction exceeded its

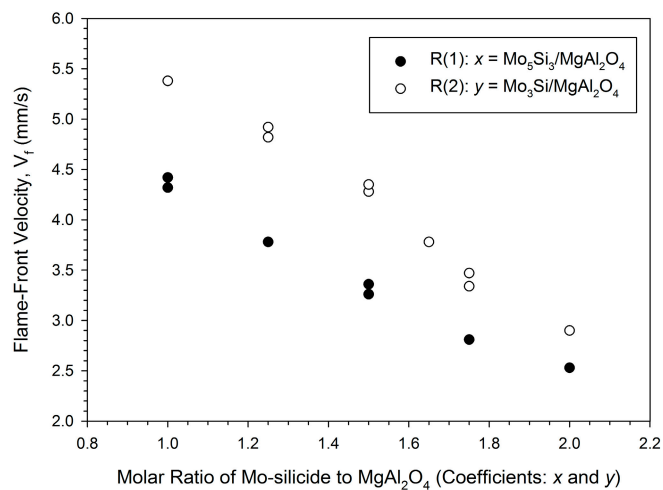
flammability limit. Nevertheless, for the powder compacts with Mo and Si lesser than a critical amount (e.g.,  $x < 1.0$  and  $y < 1.0$ ), combustion was violent and occurred almost in a manner of thermal explosion. This caused massive sample melting and difficulty in characterization of the combustion wave. Therefore, the scope of experimental variables conducted by this study was set stoichiometric coefficients ( $x$  and  $y$ ) between 1.0 and 2.0.

Figure 2 shows a decrease in the combustion wave velocity with increasing silicide content for both reaction systems. The combustion wave velocity roughly ranges between 2.5 and 5.4 mm/s. As stated earlier, the increase of Si and Mo powders in the samples has a cooling effect on combustion. Formation of  $\text{Mo}_5\text{Si}_3$  in Reaction (1) requires larger amounts of Mo and Si than the synthesis of  $\text{Mo}_3\text{Si}$  in Reaction (2). Consequently, at equal stoichiometric coefficients, Reaction (2) shows a higher combustion front velocity than Reaction (1).

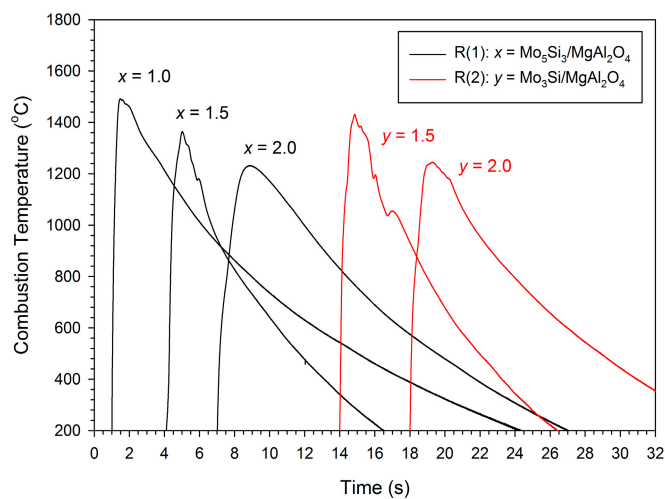


**Figure 1.** Self-propagating combustion images recorded from (a) Reaction (1) with  $x = 1.5$  and (b) Reaction (2) with  $y = 1.75$ .

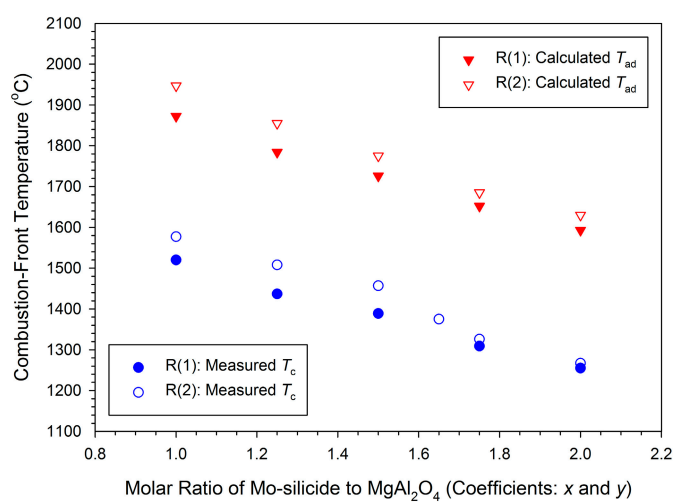
Typical combustion temperature profiles presenting the reaction exothermicity of different powder compacts are plotted in Figure 3a. The temperature profiles feature a sudden rise, signifying a rapid arrival of the combustion wave, and the pinnacle representing the combustion front temperature ( $T_c$ ). A substantial temperature decline after the passage of combustion wave is a result of heat loss to the surroundings. Based on the estimation of Equation (4), the radiation correction for the measured combustion front temperatures is in the range of 23–28 °C, which is more significant in the regions of higher temperatures. Figure 3b shows the variation of combustion front temperature with stoichiometric coefficients of Reactions (1) and (2). As indicated in Figure 3b, for Reaction (1), the increase of  $x$  from 1.0 to 2.0 lowers the measured combustion front temperature from 1520 to 1255 °C, which confirms the dilution effect on combustion by increasing Si and Mo. Similar decline of the reaction zone temperature was observed for Reaction (2), which shows a decrease of  $T_c$  from 1577 to 1267 °C with an increase of  $y$  from 1.0 to 2.0. It should be noted that at equal stoichiometric coefficients, the combustion front temperature of Reaction (2) is higher than that of Reaction (1).



**Figure 2.** Effect of molar ratio of Mo-silicide to  $MgAl_2O_4$  on flame-front velocities of Reactions (1) and (2).



(a)



(b)

**Figure 3.** Effect of molar ratio of Mo-silicide to  $MgAl_2O_4$  on combustion temperatures of Reactions (1) and (2): (a) Typical temperature profiles and (b) combustion front temperatures.

The calculated adiabatic combustion temperatures are also presented in Figure 3b and signify a decline with increasing stoichiometric coefficients for both reaction systems. The values of  $T_{ad}$  decrease from 1872 to 1593 °C for Reaction (1) and 1947 to 1630 °C for Reaction (2). This means that the exothermicity of Reaction (2) is higher than that of Reaction (1). Although the  $\text{MoO}_3 + 2\text{Al}$  reaction is highly energetic, the synthesis of  $\text{Mo}_5\text{Si}_3$  and  $\text{Mo}_3\text{Si}$  from solid-phase combustion is weakly exothermic. According to Merzhanov [32], the adiabatic combustion temperatures associated with formation of  $\text{Mo}_5\text{Si}_3$  and  $\text{Mo}_3\text{Si}$  are as low as 1457 and 1547 °C, respectively. Moreover, the heat capacity of  $\text{MgAl}_2\text{O}_4$  is larger than  $\text{Al}_2\text{O}_3$  [25], and pre-added  $\text{MgO}$  acts as a diluent of combustion. That is, the production of  $\text{MgAl}_2\text{O}_4$  and  $\text{Mo}_5\text{Si}_3$  or  $\text{Mo}_3\text{Si}$  imposed a cooling effect on the  $\text{MoO}_3 + 2\text{Al}$  reaction.

When compared with the measured combustion front temperatures reported in Figure 3b, the calculated values are higher by about 350 °C. It is believed that during the SHS process, the burning sample experienced substantial heat losses to the surrounding argon gas by conduction, by convection, or by both, and to the chamber wall by radiation, which resulted in the actual combustion temperature lower than the adiabatic value.

According to combustion wave kinetics [33,34], the activation energy ( $E_a$ ) of solid-phase combustion can be deduced from the correlation between  $\ln(V_f/T_c)^2$  and  $1/T_c$  in a form of linear relationship. Based on Arrhenius kinetics of the solid-state reaction, the activation energy is dependent on the reaction mechanism. Figure 4 plots the correlation of two sets of experimental data with their individual best-fitted linear lines. From the slopes of the linear lines,  $E_a = 68.8$  and  $63.8$  kJ/mol were deduced for Reactions (1) and (2), respectively. It can be seen that two activation energies are close to each other. This implies that both reactions are governed by similar reaction mechanisms, which involve aluminothermic reduction of  $\text{MoO}_3$  as the initiation step, followed by a combination of  $\text{Al}_2\text{O}_3$  and  $\text{MgO}$  to form  $\text{MgAl}_2\text{O}_4$ , and intermetallic interactions between Mo and Si to produce silicide compounds. The increase of Si and Mo in the sample reduces the combustion exothermicity, but produces no change in the reaction mechanisms. Compared with  $E_a = 54$  kJ/mol for the Al– $\text{MoO}_3$  thermite reaction [35], the synthesis reactions of this study have a higher kinetic barrier. This could most likely be caused by the fact that for Reactions (1) and (2), intermetallic and combination reactions need to continue to form  $\text{Mo}_5\text{Si}_3$  or  $\text{Mo}_3\text{Si}$  and  $\text{MgAl}_2\text{O}_4$  after reduction of  $\text{MoO}_3$  by Al. It should be noted that the actual reaction mechanism might be more complex than that proposed above, because the proceeding reactions could occur in both a sequential and parallel manner during combustion synthesis.

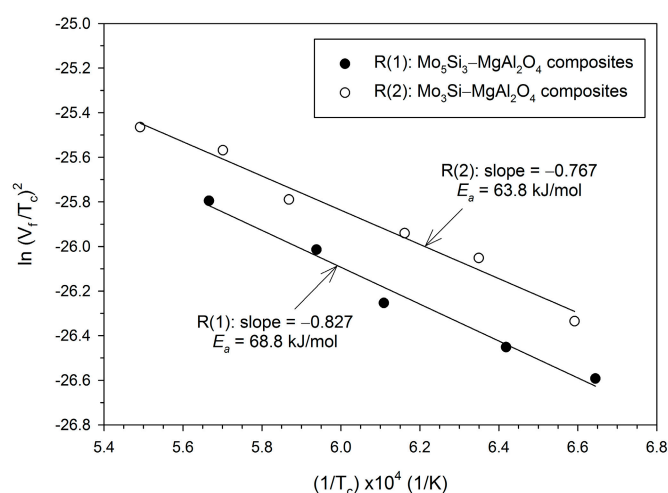


**Figure 4.** Correlation for determination of activation energies ( $E_a$ ) for formation of  $\text{Mo}_5\text{Si}_3$ – and  $\text{Mo}_3\text{Si}$ – $\text{MgAl}_2\text{O}_4$  composites from solid-phase combustion synthesis.

### 3.2. Microstructure and Composition of SHS-Derived Composites

Phase constituents of the SHS-derived composites from Reaction (1) with  $x = 1.5$  and Reaction (2) with  $y = 1.5$  are unveiled in Figure 5a,b, respectively. As shown in Figure 5a, in addition to  $\text{Mo}_5\text{Si}_3$  and  $\text{MgAl}_2\text{O}_4$  as major phases, there exist two minor species  $\text{Mo}_3\text{Si}$  and  $\text{Mo}$ . The presence of  $\text{Mo}_3\text{Si}$  could be caused by the interaction of  $\text{Mo}$  with  $\text{Mo}_5\text{Si}_3$  via  $4\text{Mo} + \text{Mo}_5\text{Si}_3 \rightarrow 3\text{Mo}_3\text{Si}$  [7]. A small amount of remnant  $\text{Mo}$  is possibly because  $\text{Mo}_5\text{Si}_3$  has a homogeneity range from 37.5 to 40% Si [36]. On the other hand,  $\text{Mo}_3\text{Si}$  is a line compound. Figure 5b shows near completion of phase conversion for Reaction (2). The as-synthesized product is a  $\text{Mo}_3\text{Si}$ – $\text{MgAl}_2\text{O}_4$  composite with a trivial amount of  $\text{Mo}$ .

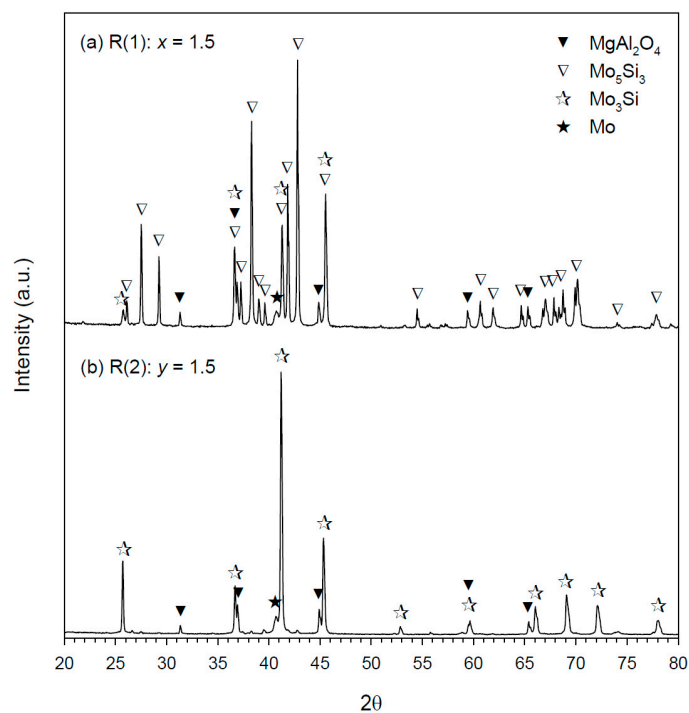


**Figure 5.** X-ray diffraction (XRD) patterns of  $\text{Mo}_5\text{Si}_3$ – $\text{MgAl}_2\text{O}_4$  and  $\text{Mo}_3\text{Si}$ – $\text{MgAl}_2\text{O}_4$  composites synthesized from (a) R(1):  $x = 1.5$  and (b) R(2):  $y = 1.5$ .

Scanning electron microscopy (SEM) micrographs in Figure 6; Figure 7 illustrate the microstructure of fracture surface of  $\text{Mo}_5\text{Si}_3$ – and  $\text{Mo}_3\text{Si}$ – $\text{MgAl}_2\text{O}_4$  composites obtained from Reactions (1) and (2), respectively. The composites display a dense and connecting morphology with embedded granular silicide particles. It is believed that the presence of liquid melt in the course of the SHS process aided in densification of the final product. As revealed in Figure 6,  $\text{MgAl}_2\text{O}_4$  crystals form a dense matrix and  $\text{Mo}_5\text{Si}_3$  grains are embedded in  $\text{MgAl}_2\text{O}_4$  or distributed over the surface. The particle size of  $\text{Mo}_5\text{Si}_3$  ranges from 2 to 10  $\mu\text{m}$ . The minor silicide phase  $\text{Mo}_3\text{Si}$  formed from Reaction (1) is not shown in Figure 6. Because most of the silicide grains were embedded in the composite and only a small amount of them were present on the fracture surface of the sample, the minor phase was sometimes difficult to find on a small area of the sample. On the other hand, the X-ray diffraction (XRD) analysis was performed with the whole specimen. Therefore, all components were identified. A similar microstructure is observed in Figure 7, showing that large  $\text{MgAl}_2\text{O}_4$  crystals are connected and small  $\text{Mo}_3\text{Si}$  grains formed from Reaction (2) have a particle size around 2–5  $\mu\text{m}$ .

EDS spectra and associated element ratios for  $\text{MgAl}_2\text{O}_4$ ,  $\text{Mo}_5\text{Si}_3$ , and  $\text{Mo}_3\text{Si}$  are also presented. In Figure 6, large connecting crystals with  $\text{Mg}:\text{Al}:\text{O} = 13.5:27.9:58.6$  are certainly  $\text{MgAl}_2\text{O}_4$  and small grains, and  $\text{Mo}:\text{Si} = 62.6:37.4$  are  $\text{Mo}_5\text{Si}_3$ . In Figure 7,  $\text{MgAl}_2\text{O}_4$  and  $\text{Mo}_3\text{Si}$  phases are determined to have  $\text{Mg}:\text{Al}:\text{O} = 13.6:28.2:58.2$  and  $\text{Mo}:\text{Si} = 76.2:23.8$ , respectively. EDS analysis confirms that atomic ratios of the compounds are very close to their stoichiometries.

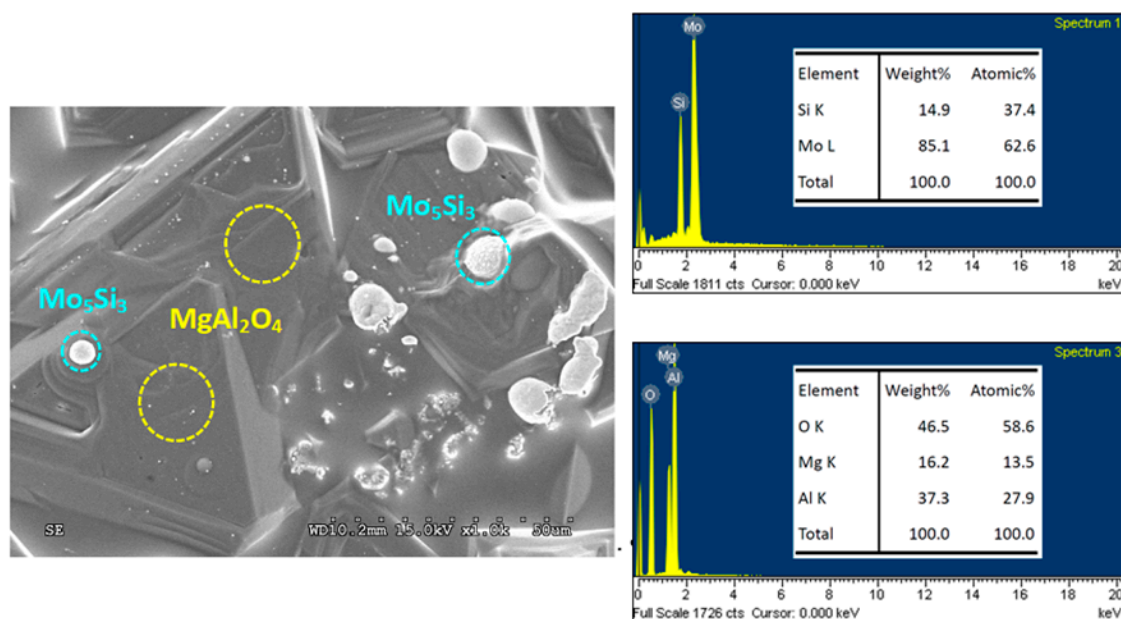


**Figure 6.** Scanning electron microscopy (SEM) micrograph and energy dispersive spectroscopy (EDS) spectra of  $\text{Mo}_5\text{Si}_3/\text{MgAl}_2\text{O}_4$  composite obtained from Reaction (1) with  $x = 1.5$ .

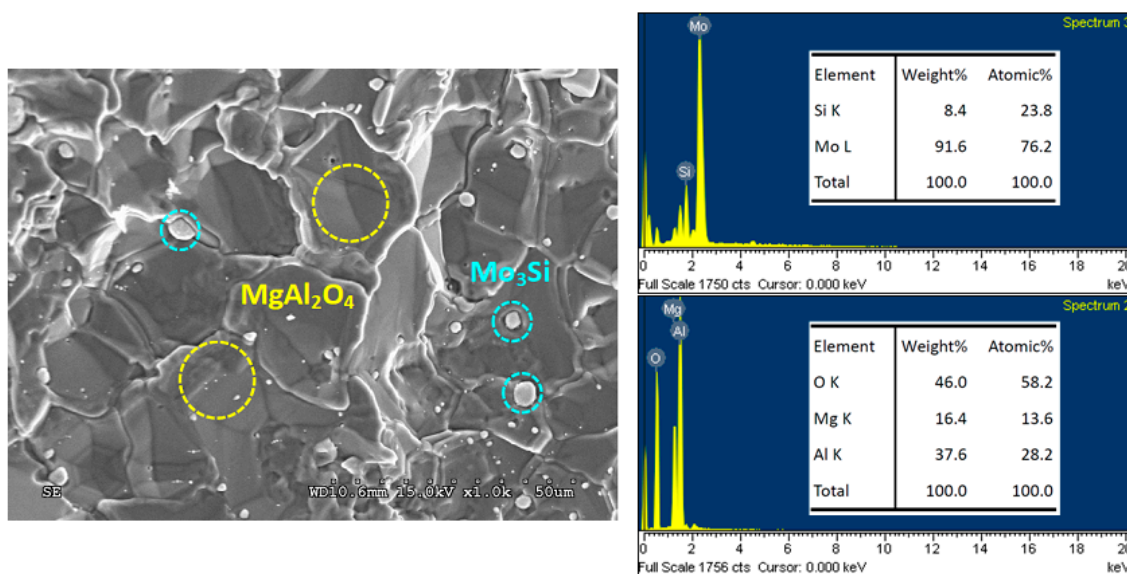


**Figure 7.** SEM micrograph and EDS spectra of  $\text{Mo}_3\text{Si}/\text{MgAl}_2\text{O}_4$  composite obtained from Reaction (2) with  $y = 1.5$ .

On account of sample melting during the SHS process, the relative density of as-synthesized composites measured by the Archimedes method reached up to 90–94%. Vickers hardness of 14.6 GPa and fracture toughness of  $6.28 \text{ MPa m}^{1/2}$  were determined for an equimolar  $\text{Mo}_5\text{Si}_3\text{--MgAl}_2\text{O}_4$  composite. Compared with pure  $\text{Mo}_5\text{Si}_3$  ( $H = 13.1 \text{ GPa}$  and  $K_{IC} = 2.37 \text{ MPa m}^{1/2}$ ) [7], the mechanical properties of  $\text{Mo}_5\text{Si}_3\text{--MgAl}_2\text{O}_4$  composite are improved. Similarly, the equimolar  $\text{Mo}_3\text{Si--MgAl}_2\text{O}_4$  composite possesses higher hardness of 13.9 GPa and fracture toughness of  $5.98 \text{ MPa m}^{1/2}$ , in comparison to single phase  $\text{Mo}_3\text{Si}$  ( $H = 13 \text{ GPa}$  and  $K_{IC} = 2\text{--}3 \text{ MPa m}^{1/2}$ ) [37].

#### 4. Conclusions

In situ formation of  $\text{Mo}_5\text{Si}_3\text{--}$  and  $\text{Mo}_3\text{Si--MgAl}_2\text{O}_4$  composites was investigated by combustion synthesis in the SHS mode. The reaction mechanisms involve metallothermic reduction of  $\text{MoO}_3$  with

Al, followed by intermetallic interactions of Si with Mo and a combination reaction of  $\text{Al}_2\text{O}_3$  with MgO. Activation energies of the solid-phase SHS reactions,  $E_a = 68.8$ , and  $63.8$  kJ/mol, were deduced from the correlation of combustion wave velocity with reaction temperature for formation of  $\text{Mo}_5\text{Si}_3$ - and  $\text{Mo}_3\text{Si}$ - $\text{MgAl}_2\text{O}_4$  composites, respectively. The increase of silicide molar content in the composite decreased the reaction exothermicity and led to flammability limits for combustion synthesis of the composites at molar ratios of  $\text{Mo}_5\text{Si}_3/\text{MgAl}_2\text{O}_4 = 2.0$  and  $\text{Mo}_3\text{Si}/\text{MgAl}_2\text{O}_4 = 2.0$ . Phase conversion from the reactants to final products was almost complete, except for small quantities of Mo and  $\text{Mo}_3\text{Si}$  remaining in the  $\text{Mo}_5\text{Si}_3$ - $\text{MgAl}_2\text{O}_4$  composite and a negligible amount of Mo in the  $\text{Mo}_3\text{Si}$ - $\text{MgAl}_2\text{O}_4$  composite. Dense products with relative density of 90–94% were obtained.  $\text{Mo}_5\text{Si}_3$  and  $\text{Mo}_3\text{Si}$  grains were embedded in the continuous  $\text{MgAl}_2\text{O}_4$  crystals. Vickers hardness of 14.6 and 13.9 GPa and fracture toughness of 6.28 and 5.98  $\text{MPa m}^{1/2}$  were determined for  $\text{Mo}_5\text{Si}_3$ - and  $\text{Mo}_3\text{Si}$ - $\text{MgAl}_2\text{O}_4$  composites, respectively. The addition of  $\text{MgAl}_2\text{O}_4$  was shown to improve the mechanical properties of  $\text{Mo}_5\text{Si}_3$  and  $\text{Mo}_3\text{Si}$ . In practice, this study demonstrated an effective fabrication route for in situ formation of  $\text{Mo}_5\text{Si}_3$ - and  $\text{Mo}_3\text{Si}$ - $\text{MgAl}_2\text{O}_4$  composites.

**Author Contributions:** Conceptualization, C.-L.Y.; methodology, C.-L.Y. and Y.-C.C.; validation, C.-L.Y. and Y.-C.C.; formal analysis, C.-L.Y. and Y.-C.C.; investigation, C.-L.Y. and Y.-C.C.; resources, C.-L.Y.; data curation, C.-L.Y. and Y.-C.C.; writing—original draft preparation, C.-L.Y. and Y.-C.C.; writing—review and editing, C.-L.Y. and Y.-C.C.; supervision, C.-L.Y.; project administration, C.-L.Y.; funding acquisition, C.-L.Y. All authors have read and agreed to the published version of the manuscript.

**Funding:** This research work was funded by the Ministry of Science and Technology of Taiwan under the grant of MOST 108-2221-E-035-026.

**Acknowledgments:** The authors are thankful for Precision Instrument Support Center of Feng Chia University in providing materials analytical facilities.

**Conflicts of Interest:** The authors declare no conflict of interest.

## References

1. Petrovic, J.J. Toughening strategies for  $\text{MoSi}_2$ -based high temperature structure silicides. *Intermetallics* **2000**, *8*, 1175–1182. [[CrossRef](#)]
2. Zhang, L.; Tong, Z.; He, R.; Xie, C.; Bai, X.; Yang, Y.; Fang, D. Key issues of  $\text{MoSi}_2$ -UHTC ceramics for ultra high temperature heating element applications: Mechanical, electrical, oxidation and thermal shock behaviors. *J. Alloys Compd.* **2019**, *780*, 156–163. [[CrossRef](#)]
3. Azim, M.A.; Christ, H.-J.; Gorr, B.; Kowald, T.; Lenchuk, O.; Albe, K.; Heilmaier, M. Effect of Ti addition on the thermal expansion anisotropy of  $\text{Mo}_5\text{Si}_3$ . *Acta Mater.* **2017**, *132*, 25–34. [[CrossRef](#)]
4. Pan, Y.; Wang, P.; Zhang, C.M. Structure, mechanical, electronic and thermodynamic properties of  $\text{Mo}_5\text{Si}_3$  from first-principles calculations. *Ceram. Int.* **2018**, *44*, 12357–12362. [[CrossRef](#)]
5. Lemberg, J.A.; Ritchie, R.O. Mo–Si–B alloys for ultrahigh-temperature structural applications. *Adv. Mater.* **2012**, *24*, 3445–3480. [[CrossRef](#)] [[PubMed](#)]
6. Abbasi, A.R.; Shamanian, M. Synthesis of  $\alpha$ -Mo– $\text{Mo}_5\text{Si}_3$ – $\text{Mo}_3\text{Si}$  nanocomposite powders by two-step mechanical alloying and subsequent heat treatment. *J. Alloys Compd.* **2011**, *509*, 8097–8104. [[CrossRef](#)]
7. Chen, H.; Ma, Q.; Shao, X.; Ma, J.; Wang, C.; Huang, B. Microstructure, mechanical properties and oxidation resistance of  $\text{Mo}_5\text{Si}_3$ - $\text{Al}_2\text{O}_3$  composites. *Mater. Sci. Eng. A* **2014**, *592*, 12–18. [[CrossRef](#)]
8. Wang, L.; Fu, Q.; Zhao, F. Improving oxidation resistance of  $\text{MoSi}_2$  coating by reinforced with  $\text{Al}_2\text{O}_3$  whiskers. *Intermetallics* **2018**, *94*, 106–113. [[CrossRef](#)]
9. Chen, H.; Shao, X.; Wang, C.Z.; Pu, X.P.; Zhao, X.C.; Huang, B.X.; Ma, J. Mechanical and wear properties of  $\text{Mo}_5\text{Si}_3$ - $\text{Mo}_3\text{Si}$ - $\text{Al}_2\text{O}_3$  composites. *Intermetallics* **2017**, *85*, 15–25. [[CrossRef](#)]
10. Ganesh, I. A review on magnesium aluminate ( $\text{MgAl}_2\text{O}_4$ ) spinel: Synthesis, processing and applications. *Int. Mater. Rev.* **2013**, *58*, 63–112. [[CrossRef](#)]
11. Ma, Y.; Liu, X. Kinetics and thermodynamics of Mg–Al disorder in  $\text{MgAl}_2\text{O}_4$ -spinel: A review. *Molecules* **2019**, *24*, 1704. [[CrossRef](#)] [[PubMed](#)]
12. Ganesh, I.; Srinivas, B.; Johnson, R.; Saha, B.P.; Mahajan, Y.R. Microwave assisted solid state reaction synthesis of  $\text{MgAl}_2\text{O}_4$  spinel powders. *J. Eur. Ceram. Soc.* **2004**, *24*, 201–207. [[CrossRef](#)]

13. Wen, Y.; Liu, X.; Chen, X.; Jia, Q.; Yu, R.; Ma, T. Effect of heat treatment conditions on the growth of MgAl<sub>2</sub>O<sub>4</sub> nanoparticles obtained by sol-gel method. *Ceram. Int.* **2017**, *43*, 15246–15253. [[CrossRef](#)]
14. Padmaraj, O.; Venkateswarlu, M.; Satyanarayana, N. Structural, electrical and dielectric properties of spinel type MgAl<sub>2</sub>O<sub>4</sub> nanocrystalline ceramic particles synthesized by the gel-combustion method. *Ceram. Int.* **2015**, *41*, 3178–3185. [[CrossRef](#)]
15. Merzhanov, A.G. Combustion processes that synthesize materials. *J. Mater. Process. Technol.* **1996**, *56*, 222–241. [[CrossRef](#)]
16. Levashov, E.A.; Mukasyan, A.S.; Rogachev, A.S.; Shtansky, D.V. Self-propagating high-temperature synthesis of advanced materials and coatings. *Int. Mater. Rev.* **2017**, *62*, 203–239. [[CrossRef](#)]
17. Liu, G.; Chen, K.; Li, J. Combustion synthesis: An effective tool for preparing inorganic materials. *Scr. Mater.* **2018**, *157*, 167–173. [[CrossRef](#)]
18. Sharifitabar, M.; Vahdati Khaki, J.; Haddad Sabzevar, M. Formation mechanism of TiC–Al<sub>2</sub>O<sub>3</sub>–Fe<sub>3</sub>Al composites during self-propagating high-temperature synthesis of TiO<sub>2</sub>–Al–C–Fe system. *Ceram. Int.* **2016**, *42*, 12361–12370. [[CrossRef](#)]
19. Ghorbantabar Omran, J.; Sharifitabar, M.; Shafiee Afarani, M. On the self-propagating high-temperature synthesis of tungsten boride containing composite powders from WO<sub>3</sub>–B<sub>2</sub>O<sub>3</sub>–Mg system. *Ceram. Int.* **2018**, *44*, 14355–14362. [[CrossRef](#)]
20. Yeh, C.-L.; Ke, C.-Y. Combustion synthesis of FeAl-based composites from thermite and intermetallic Reactions. *Crystals* **2019**, *9*, 127. [[CrossRef](#)]
21. Zaki, Z.I.; Mostafa, N.Y.; Rashad, M.M. High pressure synthesis of magnesium aluminate composites with MoSi<sub>2</sub> and Mo<sub>5</sub>Si<sub>3</sub> in a self-sustaining manner. *Ceram. Int.* **2012**, *38*, 5231–5237. [[CrossRef](#)]
22. Horvitz, D.; Gotman, I. Pressure-assisted SHS synthesis of MgAl<sub>2</sub>O<sub>4</sub>–TiAl in situ composites with interpenetrating networks. *Acta Mater.* **2002**, *50*, 1961–1971. [[CrossRef](#)]
23. Omran, J.G.; Afarani, M.S.; Sharifitabar, M. Fast synthesis of MgAl<sub>2</sub>O<sub>4</sub>–W and MgAl<sub>2</sub>O<sub>4</sub>–W–W<sub>2</sub>B composite powders by self-propagating high-temperature synthesis reactions. *Ceram. Int.* **2018**, *44*, 6508–6513. [[CrossRef](#)]
24. Yeh, C.L.; Chen, W.L. A combustion route to synthesize Mo<sub>5</sub>SiB<sub>2</sub>–Al<sub>2</sub>O<sub>3</sub> composites. *Vacuum* **2019**, *163*, 288–291. [[CrossRef](#)]
25. Binnewies, M.; Milke, E. *Thermochemical Data of Elements and Compounds*; Wiley-VCH Verlag GmbH: Weinheim, Germany, 2002; pp. 692–693.
26. Liang, Y.H.; Wang, H.Y.; Yang, Y.F.; Zhao, R.Y.; Jiang, Q.C. Effect of Cu content on the reaction behaviors of self-propagating high-temperature synthesis in Cu–Ti–B<sub>4</sub>C system. *J. Alloys Compd.* **2008**, *462*, 113–118. [[CrossRef](#)]
27. Yeh, C.L.; Chen, Y.L. An experimental study on self-propagating high-temperature synthesis in the Ta–B<sub>4</sub>C system. *J. Alloys Compd.* **2009**, *478*, 163–167. [[CrossRef](#)]
28. Bradley, D.; Matthews, K.J. Measurement of high gas temperatures with fine wire thermocouples. *J. Mech. Eng. Sci.* **1968**, *10*, 299–305. [[CrossRef](#)]
29. Holman, J.P. The Measurement of Temperature. In *Experimental Methods for Engineers*, 7th ed.; McGraw-Hill: New York, NY, USA, 2001; pp. 390–399.
30. Evans, A.G.; Charles, E.A. Fracture toughness determinations by indentation. *J. Am. Ceram. Soc.* **1976**, *59*, 371–372. [[CrossRef](#)]
31. Rios, C.T.; Coelho, A.A.; Batista, W.W.; Gonçalves, M.C.; Caram, R. ISE and fracture toughness evaluation by Vickers hardness testing of an Al<sub>3</sub>Nb–Nb<sub>2</sub>Al–AlNbNi in situ composite. *J. Alloys Compd.* **2009**, *472*, 65–70. [[CrossRef](#)]
32. Merzhanov, A.G. Solid flames: Discoveries, concepts, and horizons of cognition. *Combust. Sci. Technol.* **1994**, *98*, 307–336. [[CrossRef](#)]
33. Varma, A.; Rogachev, A.S.; Mukasyan, A.S.; Hwang, S. Combustion synthesis of advanced materials: Principals and applications. *Adv. Chem. Eng.* **1998**, *24*, 79–225.
34. Yeh, C.L.; Wang, H.J. A comparative study on combustion synthesis of Ta–B compounds. *Ceram. Int.* **2011**, *37*, 1569–1573. [[CrossRef](#)]
35. Williams, R.A.; Schoenitz, M.; Ermoline, A.; Dreizin, E.L. Low-temperature exothermic reactions in fully-dense Al/MoO<sub>3</sub> nanocomposite powders. *Thermochim. Acta* **2014**, *594*, 1–10. [[CrossRef](#)]

36. Massalski, T.B.; Okamoto, H.; Subramanian, P.R.; Kacprzak, L. *Binary Alloy. Phase Diagrams*; ASM International: Materials Park, OH, USA, 1987.
37. Rosales, I.; Schneibel, J.H. Stoichiometry and mechanical properties of Mo<sub>3</sub>Si. *Intermetallics* **2000**, *8*, 885–889. [[CrossRef](#)]



© 2019 by the authors. Licensee MDPI, Basel, Switzerland. This article is an open access article distributed under the terms and conditions of the Creative Commons Attribution (CC BY) license (<http://creativecommons.org/licenses/by/4.0/>).